Dyes and Pigments 92 (2012) 790–797

Contents lists available at ScienceDirect

Dyes and Pigments

journal homepage: www.elsevier.com/locate/dyepig

Influence of extrinsic and intrinsic parameters onto the formation of surface relief gratings in polar azo molecular glasses

Aurélie Jacquart [a], Edouard Morin [a], Feng Yang [b], Bernard Geffroy [b], Eléna Ishow [a,*]

[a] ENS Cachan, PPSM UMR CNRS 8531, 61 avenue du Président Wilson, 94235 Cachan Cedex, France
[b] LPICM-UMR CNRS 7642, CEA/IRAMIS & Ecole Polytechnique, 91128 Palaiseau, France

ARTICLE INFO

Article history:
Received 10 January 2011
Received in revised form
29 March 2011
Accepted 1 April 2011
Available online 20 April 2011

Keywords:
Molecular glasses
Azo derivatives
Photochromism
Surface relief gratings
Holography
Thin films

ABSTRACT

Polar azo derivatives exhibiting stable glass-forming properties displayed efficient migration properties as thin films when subjected to interferential illumination, and formed time-stable and rewritable surface relief gratings as high as the initial film thickness. Intrinsic (film thickness, structure bulkiness) as well as extrinsic (laser fluence and polarization) parameters dramatically influenced the rate of the relief growth as well as the maximum relief amplitude. The superimposition of +45°/−45°-polarized beams unexpectedly conducted to a diffraction efficiency ten times as high as the combination of two p/p (parallel to the incident plane) polarized beams. The introduction of bulky anthryl Diels–Alder substituents showed net increase in the modulation amplitude due to the creation of large free volume around each azo unit, facilitating the azo migration within the less densely packed material.

1. Introduction

Azo compounds, known for their strong one-photon absorption cross-section, have been used for long as dyes for textile dyes [1] and non-rewritable optical data storage [2]. In the late 80's, their photochromic properties involving a reversible *E*–*Z* photoisomerization around the N=N double bond initiated an entire field of new investigations related to their startling photomechanical capabilities [3–5]. The latter have been illustrated in photonics for the fabrication of electro-optical modulators [6], the translation of micrometric-sized objects such as liquid droplets [7,8] or polystyrene microspheres [9], and the stretching and bending of azo-functionalized liquid crystalline polymers along the direction of the impinging polarized light [10,11]. Another phenomenon whose mechanism is still highly debated relates to the bulk migration of azo moieties when subjected to interferential illumination [12,13]. It is beyond the scope of the present manuscript to describe them in detail but three main models based on asymmetric diffusion [14], mean-field theory [15,16], and isomerization pressure [17], have been proposed to explain the formation of surface relief gratings. All of them relate to the photoisomerization reaction of azo polymers whereas a new class of organic materials, involving glass-forming small molecules [18,19], could offer simpler models to assess the critical structural and electronic parameters coming into play. No chain entanglement needs to be considered while kinetic and thermodynamic characteristics linked to the independent microscopic properties of each molecule (such as the molecular volume, dipole moment, energy levels of the *E* and *Z* isomers) can be more precisely defined than for polymeric systems. Although there is a growing interest in amorphous molecular azo materials [20–23], their structure often resembles that of aminoazobenzene-like derivatives following Rau's classification [1], which makes direct comparison more delicate with the usual push–pull structure of the azo polymerized units referred as to pseudo-stilbene-like. We report herein detailed investigations of the influence of intrinsic (molecular bulkiness, film thickness) and extrinsic (light fluence and polarization) parameters onto the migration efficiency of polar azo molecules leading to perfectly time-stable and optically rewritable surface relief gratings at room temperature.

2. Materials and methods

2.1. General methods

^{1}H and ^{13}C NMR spectra were recorded on a JEOL 400 MHz spectrometer and chemical shifts were reported in ppm relative

* Corresponding author. Tel.: +33 2 5112 5375; fax: +33 2 5112 5204.
E-mail address: elena.ishow@univ-nantes.fr (E. Ishow).

0143-7208/$ – see front matter © 2011 Elsevier Ltd. All rights reserved.
doi:10.1016/j.dyepig.2011.04.001

to TMS or referenced to the residual solvent. High resolution mass spectra were obtained by MALDI-TOF (Voyager DE-STR, Applied Biosystems). Glass transition temperatures T_g were measured by using differential scanning calorimetry (Perkin Elmer Pyris Diamond) in aluminum caps under a nitrogen flow at a scan rate of 20 °C min^{-1} over the temperature range [30 °C–250 °C].

2.2. Commercial chemicals and compounds

All chemical reagents and solvents were purchased from commercial sources (Aldrich, Acros, SDS) and used as received. Spectroscopic grade toluene was used for spectroscopic measurements. All air-sensitive reactions were performed under argon using a vacuum line. Analytical thin layer chromatography was performed on Kieselgel F-254 precoated plates. Flash chromatography was carried out with silica gel from SDS. The compounds 4-nitrosobenzoic acid [24], methyl 4-nitrosobenzoate [24], bis(4′-tert-butylbiphenyl-4-yl)-4-aminophenylamine **1** [25], and 2,6-dihydroxy-9,10-dihydro-11,12-dicarbomethoxy-ethenoanthracene **4** [26] were synthesized according to literature procedures. Thin films were obtained by spin-casting chloroform solutions at various azo wt.% (1 wt.% and 2 wt.%) on pre-cleaned glass substrates at a speed comprised between 500 and 2000 rpm, and dried further under vacuum for 24 h. All solutions were systematically filtered before spin-coating with 0.45 μm porous Millex membranes purchased from Waters.

2.2.1. Synthesis of methyl 4-{4′-[bis(4′-tert-butylbiphenyl-4-yl) amino]phenylazo}benzoate ***2* AzoMe**

Methyl 4-nitrosobenzoate (80 mg, 0.48 mmol) was dissolved in glacial acetic acid (3.5 mL) under argon. Bis(4′-tert-butylbiphenyl-4-yl)-4-aminophenylamine **1** (210 mg, 0.4 mmol) was added portionwise; meanwhile the pale yellow solution turned deep brown red. After stirring at room temperature for 48 h, a fine orange product precipitated, corresponding to the pure compound **2** which was filtered off and washed thoroughly with water (95%, 250 mg). T_g 68 °C; λ_{max} (nm) [ε (mol^{-1}.L.cm^{-1})]: 465 [17900], 330 [29600]; ^{1}H NMR (400 MHz, $CDCl_3$, TMS): (ppm) = 8.16 (d, ^{3}J(H,H) = 8.2 Hz, 2H), 7.90 (d, ^{3}J(H,H) = 8.7 Hz, 2H), 7.86 (d, ^{3}J(H,H) = 8.2 Hz, 4H), 7.56 (d, ^{3}J(H,H) = 8.2 Hz, 4H), 7.54 (d, ^{3}J(H,H) = 8.2 Hz, 4H), 7.46 (d, ^{3}J(H,H) = 8.7 Hz, 4H), 7.27 (d, ^{3}J(H,H) = 8.7 Hz, 4H), 7.21 (d, ^{3}J(H,H) = 8.7 Hz, 2H), 3.95 (s, 3H, $-CO_2CH_3$), 1.37 (s, 18H, −tBu); ^{13}C NMR (100 MHz, $CDCl_3$, TMS): (ppm) = 166.8, 159.8, 155.7, 150.3, 147.3, 145.7, 137.6, 137.2, 131.1, 130.7, 128.2, 126.6, 125.95, 125.92, 124.9, 122.4, 121.6, 52.4, 34.7, 31.5; HRMS (MALDI-TOF), m/z [M^+]: for $C_{46}H_{45}N_3O_2$ calculated 671.3512; found 671.35063.

2.2.2. Synthesis of 4-{4′-[bis(4′-tert-butylbiphenyl-4-yl)amino] phenylazo}benzoic acid ***3***

4-Nitrosobenzoic acid (570 mg, 3.82 mmol) was dissolved in a 1:1 DMSO:glacial acetic acid (52 mL) mixture under argon. Bis(4′-tert-butylbiphenyl-4-yl)-4-aminophenylamine **1** (1.0 g, 1.91 mmol) was added portionwise; meanwhile the pale yellow solution turned deep brown red. After stirring at room temperature for 48 h, a fine red product precipitated, corresponding to the pure acid **3** which was filtered off and washed thoroughly with water (95%, 1.2 g). T_m = 108 °C; ^{1}H NMR (400 MHz, $CDCl_3$, TMS): (ppm) = 8.22 (d, ^{3}J(H,H) = 8.7 Hz, 2H), 7.93 (d, ^{3}J(H,H) = 8.2 Hz, 2H), 7.88 (d, ^{3}J(H,H) = 8.7 Hz, 2H), 7.56 (d, ^{3}J(H,H) = 8.2 Hz, 4H), 7.55 (d, ^{3}J(H,H) = 8.7 Hz, 4H), 7.47 (d, ^{3}J(H,H) = 8.2 Hz, 4H), 7.27 (d, ^{3}J(H,H) = 8.7 Hz, 4H), 7.21 (d, ^{3}J(H,H) = 8.7 Hz, 2H), 1.37 (s, 18H, −tBu); HRMS (MALDI-TOF), m/z [M+] for $C_{45}H_{43}N_3O_2$ calculated 657.3355; found 657.3349.

2.2.3. Synthesis of 4-[bis(4′-tert-butylbiphenyl-4-yl)amino]-4′-([(6-hydroxy-9,10-dihydro-11,12-dicarbomethoxy-etheno)anthracene-2-yl]oxycarbonyl)azobenzene ***5* AzoDA** [27]

To a solution of 2,6-dihydroxy-9,10-dihydro-11,12-dicarbomethoxy-ethenoanthracene **4** (200 mg, 0.56 mmol) in anhydrous dichloromethane (200 mL) was slowly added a solution of acid **3** (184 mg, 0.28 mmol), dimethylaminopyridinium *p*-toluenesulfonate (DPTS) (26 mg, 0.08 mmol) and diisopropylcarbodiimide (DIPC) (53 mg, 0.42 mmol) dissolved in anhydrous dichloromethane (100 mL). The reaction mixture was allowed to stir at reflux overnight. Concentration under vacuum followed by silica gel column chromatography using petroleum ether/ethyl acetate 7/3 as an eluent, afforded **5** as a deep red solid (65%, 180 mg). T_g 123 °C; UV–vis (toluene), λ_{max} (nm) [ε (mol^{-1} L cm^{-1})]: 474 [22800], 328 [29600]; ^{1}H NMR (400 MHz, $CDCl_3$, TMS): (ppm) = 8.27 (d, ^{3}J(H,H) = 8.7 Hz, 2H), 7.94 (d, ^{3}J(H,H) = 8.7 Hz, 2H), 7.88 (d, ^{3}J(H,H) = 9.1 Hz, 2H), 7.56 (d, ^{3}J(H,H) = 8.2 Hz, 4H), 7.28–7.19 (m, 8H), 6.92 (d, ^{4}J(H,H) = 2.3 Hz, 1H), 6.88 (dd, ^{4}J(H,H) = 2.3 Hz, ^{3}J(H,H) = 7.7 Hz, 1H), 6.45 (dd, ^{4}J(H,H) = 2.3 Hz, ^{3}J(H,H) = 7.7 Hz, 1H), 5.40 (s, 1H), 3.80 (s, 3H, $-CO_2CH_3$), 3.79 (s, 3H, $-CO_2CH_3$), 1.37 (s, 18H; −tBu); ^{13}C NMR (100 MHz, $CDCl_3$, TMS): (ppm) = 166.06, 165.99, 164.97, 156.03, 153.75, 151.19, 150.21, 148.27, 147.52, 147.10, 146.75, 145.95, 145.46, 145.24, 141.28, 137.40, 137.14, 134.92, 131.19, 129.98, 128.03, 126.45, 125.84, 125.77, 124.88, 124.55, 125.35, 122.48, 121.36, 117.98, 117.59, 112.18, 111.30, 52.54, 51.85, 51.56, 34.53, 31.35; HRMS (MALDI-TOF), m/z [M^++H]: for $C_{65}H_{57}N_3O_7H$ calculated 992.4275; found 992.4269.

2.3. Experimental techniques

All comparative photoisomerization and holographic photomigration experiments involving **AzoMe** and **AzoDA** were performed on isoabsorbing solutions or thin films to avoid artifact interpretations.

2.3.1. Absorption spectroscopy and kinetic studies

UV–vis absorption spectra in solution and thin films were measured with a Varian spectrophotometer (model Cary 500).

The *E*–*Z* photoisomerization reaction was induced in toluene solution by means of a continuous white light Hg–Xe source (Hamamatsu, Model LC8) equipped with a quartz optical guide and a narrow bandpass filter at 485 nm, and in thins films by means of a continuous wave argon ion laser working at 488 nm as a pump source. Kinetics of the *Z*–*E* back thermal relaxation was recorded on samples in the photostationary state, by following the absorbance change at specific wavelengths. Rate constants k_i were determined by modeling the back thermal reaction in fluid solution and thin films with a monoexponential fit $a \times \exp(-kt)$ and a biexponential fit $a_1 \times \exp(-k_1 t) + a_2 \times \exp(-k_2 t)$ respectively.

2.3.2. Holographic setup and refractive index measurements

Holographic inscriptions were carried out on spin-coated thin films by means of a two-arm interferometer setup splitting an Ar^+ laser beam working at 488 nm into two coherent beams of equal intensity. Polarization and fluence were varied with regard to the experiments to be performed. Interference gratings were obtained with a spatial period Λ = 1.40 μm in accord with the bissecting incident angle $\theta = 10°$ between both interfering beams following Bragg's diffraction law $\wedge = \lambda/2\sin(\theta)$. Surface relief grating (SRG) height measurements were carried out by using a Veeco Explorer atomic force microscope working in a tapping mode. Formation of SRGs was followed *in situ* by recording the first diffracted order of a low-power He–Ne laser (1.9 mW) working at 632.8 nm by means of a photodiode detector (Ophir – PD300 and PD300 UV heads) (Fig. 1).

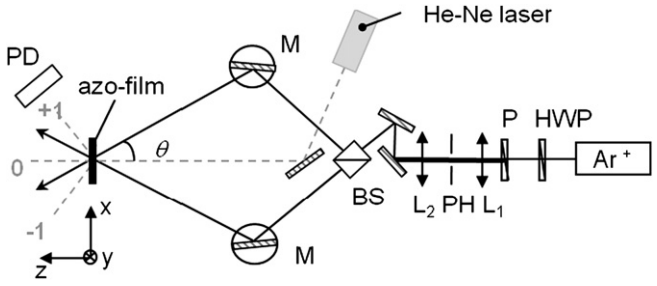

Fig. 1. Holographic setup for SRG recording: HWP, half-wave plate; P, polarizer; L_1, lens f50; PH, pinhole (∅ 25 μm); L_2, lens f150; BS, cube beam-splitter; M, mirror; PD, photodetector; Ar^+, argon ion laser working at 488 nm; He–Ne laser working at 633 nm (spot diameter of 2 mm).

Refractive index measurements were performed by ellipsometry using a spectroscopic ellipsometer Jobin-Yvon-Horiba UVISEL-SE working from the UV to NIR range (250–1100 nm). Thickness measurements were independently performed by means of a Dektak 6M stylus profilometer (Veeco).

3. Results and discussion

3.1. Synthesis and thermal properties

The introduction of different ester moieties allows for the straightforward variation of group bulkiness without affecting the charge transfer within the generic backbone. Keeping the absorption maximum wavelengths and molar absorption coefficients almost similar from one compound to another is of high importance for comparative purposes since the photoisomerization efficiency and consequently the extent of photomigration are primarily ruled by the absorbed quantum energy as well as the energy levels of both the *E* and *Z* isomers. We then chose the triphenylamino unit as an electron-donating moiety not only for its stronger donating properties compared to hydroxyl or ether units but also for its twisted geometry impairing strong intermolecular interactions. The latter were reduced by the introduction of two peripheral tert-butylphenyl subsituents, which yielded amorphous materials as revealed by thermal analyses (*vide infra*). In order to assess the influence of additional steric crowding and/or larger free volume created around the azo derivatives, we introduced the 2,6-dihydroxy-9,10-dihydro-11,12-dicarbomethoxy-ethenoanthracenyl moiety at the ester unit. Swager et al. showed that anthryl Diels–Alder (DA) adduct moieties substituting semi-conjugated polymers led to highly porous materials, hence analyte diffusion for sensing applications or chain organization for mechanically-resistant stretchable materials were much facilitated [28].

We adopted a modular synthesis involving the condensation between the appropriate nitroso derivatives and the primary aromatic amine bis(4′-*tert*-butylbiphenyl-4-yl)-4-aminophenylamine **1**, obtained after reduction of the corresponding nitro compound by hydrazine in the presence of charcoal-supported palladium(0) (Scheme 1).

Following this pathway, both the carboxylic acid and the corresponding methyl ester derivative were obtained in excellent yields of about 95% as bright red and orange pure precipitates, respectively, with no need of further purification except thorough washing of the powders with water. This method is even more appropriate for the carboxylic acid compound which was further engaged in a mild monoesterification process, assisted by diisopropylcarbodiimide in the presence of dimethylaminopyridinium *p*-toluenesulfonate, with the DA biphenol **1** used in a twofold excess, to limit diesterification. The monoester was very easily separated by silica gel column chromatography from the diester side-product and the unreacted reagents due to their much distinct adsorption properties.

Differential scanning calorimetry measurements showed, for both esters, a clear second-order transition characteristic of a glass transition at a temperature $T_g = 68$ °C and 123 °C for **AzoMe** and **AzoDA** respectively. No further recrystallization peaks were observed at higher temperatures, ensuring time-stable glass-forming properties for the azo materials. The T_g value for **AzoDA**, twice as high as that for **AzoMe**, stems from the presence of the bulky anthryl DA adduct creating larger internal geometrical constraints and less apparent “fluidity”. Contrary to the intuitive perception, steric crowding does not necessarily reduce the efficiency of bulk migration as demonstrated below.

3.2. UV–vis absorption spectroscopy and photochromic studies

All comparative experiments were performed on isoabsorbing solutions or thin films to avoid artifact interpretations. Both

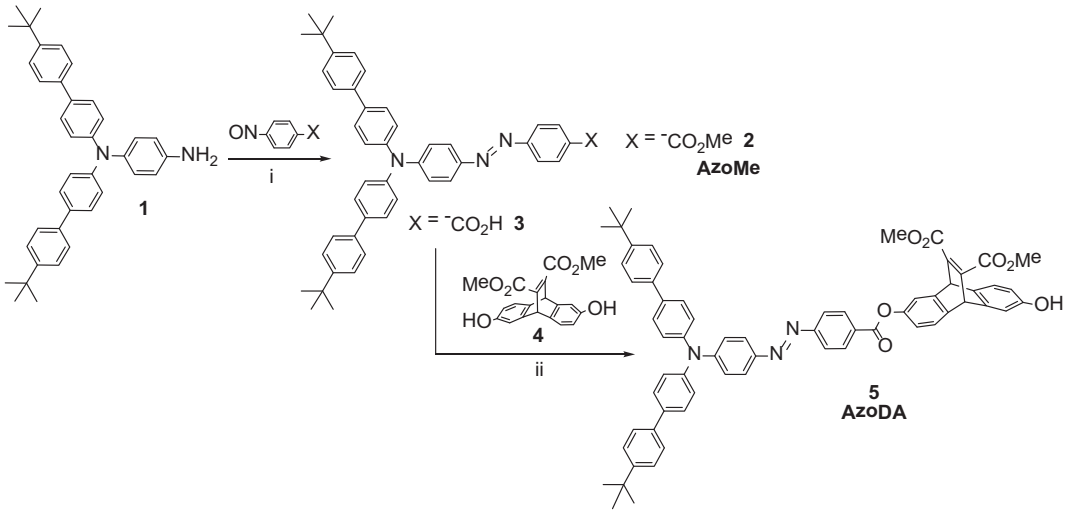

Scheme 1. Synthetic pathway to the glass-forming azo esters **AzoMe** and **AzoDA**. i) 4-nitrosobenzoic acid or methyl 4-nitrosobenzoate, acetic acid:DMSO 1:1 or acetic acid, RT, 48 h, 95%. ii) 2,6-dihydroxy-9,10-dihydro-11,12-dicarbomethoxy-ethenoanthracene, dimethylaminopyridinium *p*-toluenesulfonate, diisopropylcarbodiimide, anhydrous dichloromethane RT, 12 h, 65%.

Table 1
Thermal and UV–vis spectroscopic properties of **AzoMe** and **AzoDA** in toluene solution (5×10^{-5} mol L^{-1}) and as 200 nm-thick films.

Compound	T_g [°C][a]	λ_{max}(abs) [nm] (ε [mol^{-1} L cm^{-1}]) in solution	λ_{max}(abs) [nm] thin films[b]
AzoMe	68	465 (17900), 330 (26600)	471
AzoDA	123	473 (22800), 328 (29600)	474

[a] Measured by DSC using a 20 °C min^{-1} thermal gradient.
[b] Spin-cast from 2 wt.% chloroform solutions and dried under vacuum for 24 h.

Table 2
Kinetic components of the back thermal relaxation **AzoMe** and **AzoDA** in toluene solution (5×10^{-5} mol L^{-1}) and as spin-coated thin films (200 nm-thick) irradiated to the photostationary state.

Compound	Solution[a]		Thin film[b]				
	k [10^{-5} s^{-1}]	ρ_{min} [%][c]	k_1 [10^{-5} s^{-1}]	f_1	k_2 [10^{-5} s^{-1}]	f_2	ρ_{min} [%][c]
AzoMe	8	50	3.3	92	21	8	21
AzoDA	9.8	47	2.4	97.5	37	2.5	16

[a] First-order kinetics.
[b] Biexponential fit $a_1\exp(-k_1t) + a_2\exp(-k_2t)$ with $k_i = 1/\tau_i$ and normalized fractions defined as $f_i = a_i\tau_i/(a_i\tau_i + a_j\tau_j)$.
[c] Minimum photoconversion yield $E \rightarrow Z$ (assuming that the Z form is not absorbing at 465 nm) obtained by irradiation at 465 nm (30 mW cm^{-2}).

compounds exhibited very similar absorption properties in solution and in the solid state with a first band in the UV range involving biphenyl-centered transition and a second band in the visible around 465 nm (471 nm) and 473 nm (474 nm) for toluene solutions (spin-coated thin films) of **AzoMe** and **AzoDA** respectively (Table 1) [27].

Irradiation with a continuous mercury–xenon lamp equipped with an optical fiber and a narrow bandpass filter at 485 nm led to a significant decrease of the maximum in the visible region attributed to the formation of the corresponding *Z* isomers. In the first assumption of non-absorbing *Z* isomers at 485 nm, the minimum photoconversion yield ρ_{min} was estimated to be 50% and 47% for **AzoMe** and **AzoDA** in toluene, respectively (Fig. 2).

Once the photostationary state has been reached, the thermal back relaxation of the *Z* forms into the *E* isomers occurring at room temperature in the dark could be modeled by a monoexponential law $[Z] = [Z]_0\exp(-kt)$ in accord with fluid environments. The rate constants k were found to be equal to 8×10^{-5} s^{-1} and 9.8×10^{-5} s^{-1} for **AzoMe** and **AzoDA** respectively (Table 2). Given the very similar absorption spectra, photoconversion yields ρ_{min} and *Z* thermal decays for both azo esters in solution, it is clear that the DA adduct does not impact the electronic properties of the azo unit and lets the azo photoisomerization behavior almost unchanged. Photochromic discrepancy in the solid state, if any, would thus mainly originate from large geometrical rather than electronic effects. We indeed measured a lower photoconversion yield ρ_{min} for **AzoDA** which dropped down to 16%, namely one quarter less than that for **AzoMe** which was found to be 21%. Similar differences were observed for the back thermal relaxation rate constants k_i, emphasizing the existence of steric constraints. After fitting the experimental data with a double exponential law, two rate constants were determined. The slower components k_1, valued at 3.3×10^{-5} s^{-1} and 2.4×10^{-5} s^{-1} for compounds **AzoMe** and **AzoDA**, represent the major relaxation regime (Table 2). By contrast, the faster components k_2, which are larger than those in solution and attributed to very unstable *Z* geometries due to environmental constraints, were found to be 2.1×10^{-4} s^{-1} and 3.7×10^{-4} s^{-1} for compounds **AzoMe** and **AzoDA**. All of these data converge toward stiffer surroundings around the azo unit linked to the DA adduct, hence unstabilized *Z* isomers revert back even faster than the isomers of the unsubstituted azo ester only for steric reasons. We will see later that this bulkiness is actually responsible for the dramatically enhanced height modulation of the surface relief gratings.

3.3. Formation of surface relief gratings and influence of extrinsic and intrinsic parameters

Holographic irradiation using a two-beam interferometer setup was first performed on thin films of unsubstituted azo ester **AzoMe**. Three sets of parameters were explored, namely the polarization, the power as well the film thickness to assess their influence onto the process efficiency of surface relief grating formation. AFM measurements were performed immediately after the illumination process. Formation of the surface relief gratings was followed *in situ* by recording the first diffracted order of a low-power He–Ne laser (1.9 mW) working at 632.8 nm. The diffraction efficiency η was defined as follows: $\eta = 2\ I_{\pm1}/I_0$ with I_0 and $I_{\pm1}$ related to the energies of the incident beam and the first-order diffracted beam respectively of the He–Ne laser.

3.3.1. Influence of the laser polarization

We first investigated three polarization settings: s/s, p/p and +45°/−45° generating respectively pure intensity gratings, mainly intensity gratings largely modulated along the grating vector direction with a small amount of polarization variation, and mainly polarization grating with an irradiation intensity nearly constant (Fig. 3).

The film thickness was kept constant at 270 nm while the intensity for each laser beam was set at 160 mW cm^{-2} (15 mW). As

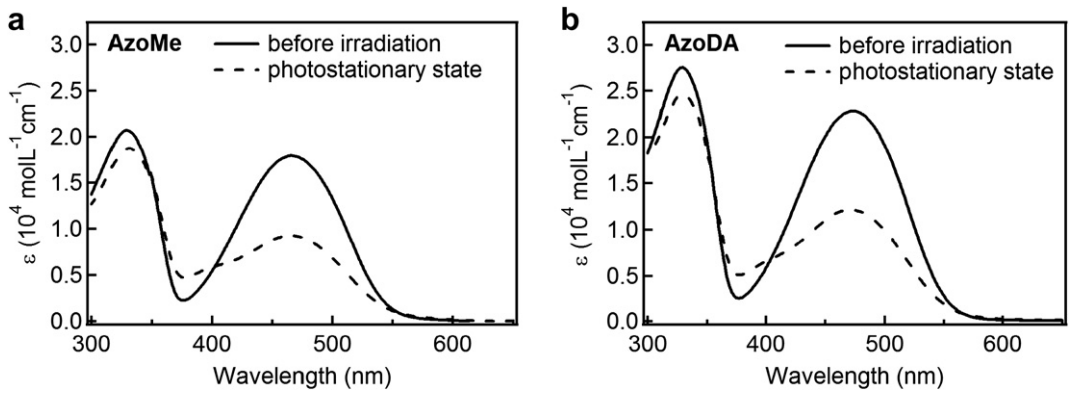

Fig. 2. UV–vis absorption spectra in toluene before irradiation and at the photostationary state reached upon irradiation at 485 nm a) **AzoMe**. b) **AzoDA**.

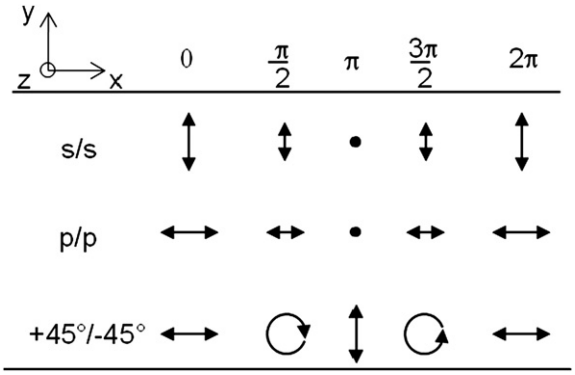

Fig. 3. Electric field vector distribution at the sample surface for three sets of polarization. The coordinate system of the electric field vector, corresponds to the coordinate system.

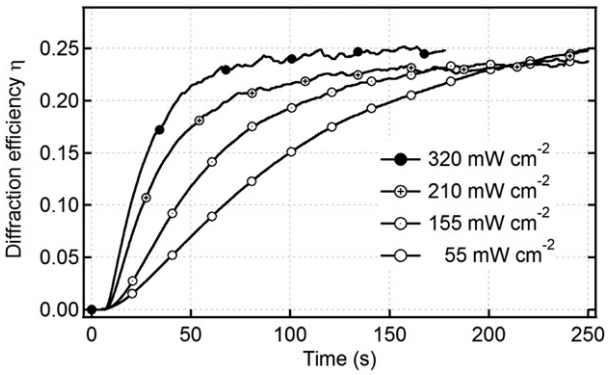

Fig. 5. Evolution of the diffraction efficiency for a 230 nm-thick **AzoMe** thin film subjected to various incident intensities for each Ar^+ laser beam fixed with a +45°/−45° polarization configuration (λ_{irr} = 488 nm).

commonly observed for the formation of SRGs, the s/s configuration creates very weak gratings less than 10 nm high with a maximum diffraction efficiency hardly reaching 0.05%. By contrast, SRGs written with p/p (where p features light polarization parallel to the incident plane) and +45°/−45° configurations generated a first-order diffraction efficiency two to four orders of magnitude larger, namely 2.8% and 20% respectively (Fig. 4).

These results strongly contrast with those commonly reported for azo polymers and several molecular glasses where both configurations yielded SRGs with similar modulation heights, albeit diffracting more efficiently for p/p with regard to +45°/−45°-polarized beams. Straight comparisons with other studies are however sometimes rather difficult since the experimental conditions in terms of irradiation powers and film thicknesses can differ considerably. In our condition, 270 nm-thick films exhibited absorbance close to 1, which lets suspect a homogeneous laser absorption throughout the sample in contrast with 50 μm-thick samples where deep layers, screened by the top layers, obviously undergo a less efficient photoisomerization reaction [22].

3.3.2. *Influence of the laser intensity*

All experiments were performed onto 230 nm-thick films. The polarized configuration was fixed at +45°/−45°; both laser beams were of equal intensity and tuned between 55 mW cm^{-2} (5 mW), 105 mW cm^{-2} (10 mW), 210 mW cm^{-2} (20 mW), and finally 320 mW cm^{-2} (30 mW) (Fig. 5).

As already reported on azo polymers, a higher irradiation power speeds up the SRG growth rate [29]. Surprisingly, in our case the maximum heights achievable were the same, and measured to be 170 nm. It is worth noting that a high diffraction efficiency of almost 25% could be reached in less than 100 s up to 250 s for the lowest intensity regime, which contrasts with the saturation obtained with polymers usually achieved after 1200 s and longer.

3.3.3. *Influence of the film thickness*

We finally studied the influence of the film thickness which was reported to dramatically impact the migration inscription rate for azo polymers on grounds of surface tension effects. For the latter, in the framework of the photomechanical effect model based on the existence of pressure gradient, migration was assumed to follow a laminar flow model described by Eq.(1), derived from the Navier–Stokes relationship [30,31]:

$$\frac{\partial h}{\partial t} = \frac{1}{3}\frac{h^3}{\eta_v}\frac{\partial^2 P(x)}{\partial x^2} \quad (1)$$

where h refers to the initial film thickness, η_v to the kinematic viscosity and P to the internal pressure.

In order to keep a uniform irradiation across the samples, we considered the following three thicknesses: 100 nm, 180 nm and 250 nm. The irradiation conditions were set at +45°/−45° with an equal intensity of 15 mW cm^{-2} for both beams. For all samples, the modulation heights were found by AFM measurements close to the initial film thickness, and reached 130 nm, 190 nm and 260 nm from the thinner to the thicker film samples (Fig. 6a).

No change in the periodic sinusoidal structure was observed with a periodic spacing invariably measured at 1.40 μm (Fig. 6b). The diffraction efficiency also increased with the film thickness in accord with deeper SRG peak-to-trough amplitudes. Finally the maximum inscription rate defined as the slope of the holographic growth curve appeared very sensitive to the initial thickness, and changes one order of magnitude from the thinner sample to the thicker one (Fig. 7). The graphical representation of the experimental rate as a function of the thickness showed a positive curvature which could be nicely modeled by a 3rd order polynomial fit following the cubic rate dependence on the initial film thickness.

This curvature contrasts with the negative curvature and the restricted amplitude of the growth rate variation for azo polymeric

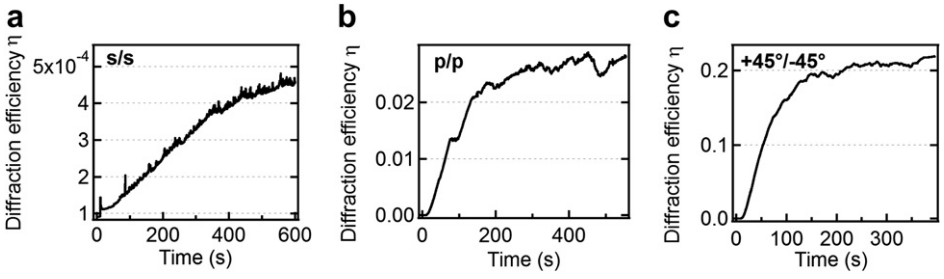

Fig. 4. Evolution of the diffraction efficiency of 270 nm-thick **AzoMe** thin films subjected to various polarization configurations of two 160 mW cm^{-2} interfering Ar^+ laser beams (λ_{irr} = 488 nm). Configuration: a) s/s (η = 0.048%); b) p/p (η = 2.8%); c) +45°/−45° (η = 20%).

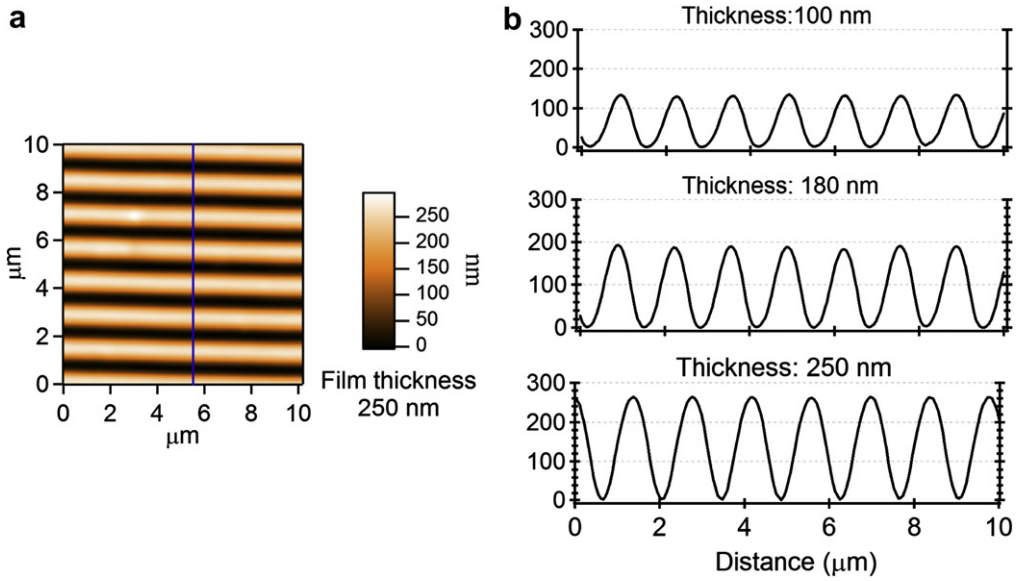

Fig. 6. AFM measurements of surface reliefs gratings written on **AzoMe** thin films using a +45°/−45° configuration with a 160 mW cm^{-2} incident intensity for each Ar^{+} laser beam. a) AFM imaging for a 250 nm-thick film. b) Z-profile for various film thicknesses.

films thicker than 100 nm [30,31]. For azo polymers, it has been reported to scale with the cube of the initial thickness *h*, and progressive deviations appeared for samples thicker than 100 nm due to marked difference in pressure/tension effects between the substrate interface and the film surface. The high sensitivity observed for the azo molecular glasses is likely to stem from the absence of long chains creating multiple anchoring points on the glass substrate as encountered for polymer chains where bulk mass transport undergoes strong acceleration for thin thicknesses until the chains are no longer in contact with the substrate surface or entangled with polymer chain interacting with the latter.

3.3.4. Photorewritability

We investigated the rewritability of the surface relief gratings previously written onto a 270 nm-thick **AzoMe** thin films. To this aim, a series of three writing–erasure cycles was performed displaying nice reversible modulations of the diffraction efficiency (from 20% to less than 0.2%) and relief height (from 280 nm to less than 10 nm), with a slight 2.5% increase of the diffraction efficiency from one cycle to another (Fig. 8).

This slight increase could be ascribed to small plasticization effects due to global disorganization of the azo molecules in surface after photoisomerization. While the writing step involved two 45°/−45°-polarized interfering beams with each a 160 mW cm^{-2} incident intensity, the erasure step involved homogenous irradiation using only one 45°-polarized beam with a twofold intensity of 320 mW cm^{-2}, which was shown to be very efficient. Under such conditions, the diffraction efficiency saturated (vanished) after an exposure period of 420 s (700 s) for the writing (erasure) step, which corresponds to a growth (disappearance) rate constant of 2.80×10^{-2} s^{-1} (1.56×10^{-2} s^{-1}). Erasure requires more stringent conditions than writing in terms of beam energy and irradiation time, which has already been noted for other polar azo molecular glasses, and ascribed to poled molecules whose rotational and translational disorientation needs repeated cycles of *Z*–*E* photoisomerization, especially for azo units with less push–pull character compared to that of nitro-containing derivatives like Disperse Red 1 [32].

3.3.5. Influence of the azo bulkiness

Thin films were made from **AzoMe** and **AzoDA** solutions in chloroform with identical azo mass concentrations (2% wt. both) to avoid differences in light absorption, which in turn would influence the migration dynamics and efficiency. Both compounds indeed exhibit close molar absorption coefficients in solution. Provided that the absorption properties in solution and in the solid state are alike, the molecular quantities of photoactive units can be

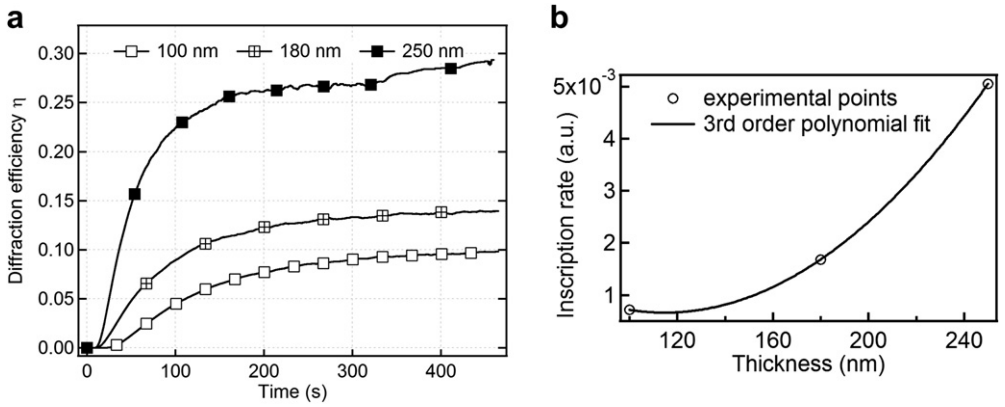

Fig. 7. a) Evolution of the diffraction efficiency for various thicknesses of **AzoMe** thin films subjected to a 160 mW cm^{-2} incident intensity for each Ar^{+} laser beam fixed in a +45°/−45° polarization configuration (λ_{irr} = 488 nm). b) Inscription rate as a function of the film thickness.

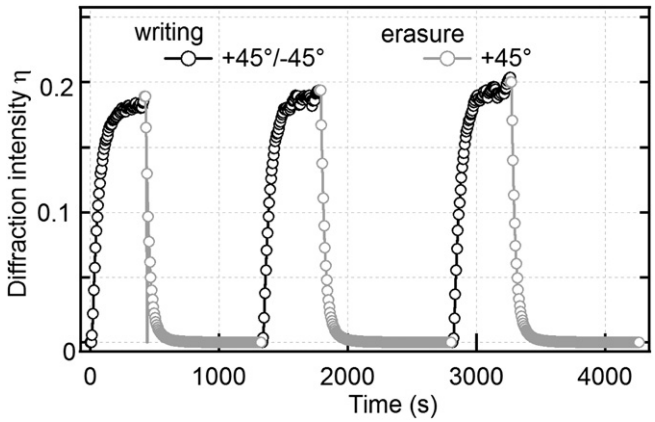

Fig. 8. Writing–erasure cycles for surface relief gratings formed on a 270 nm-thick **AzoMe** thin film. Writing involves two-beams interferential illumination with a +45°/−45° polarization configuration (160 mW cm^{-2} intensity per beam, $\lambda_{irr} = 488$ nm). Erasure involves one-beam (45°-polarized) homogenous illumination (320 mW cm^{-2} intensity, $\lambda_{irr} = 488$ nm).

considered the same. Thin film absorbances were indeed found to be very close at 1.07 and 1.14 for **AzoMe** and **AzoDA** respectively at the laser radiation wavelength ($\lambda_{max} = 488$ nm). The beam incident intensity was fixed at 15 mW cm^{-2} while a +45°/−45° polarization configuration, proved the most efficient one in our experimental investigations, was again adopted.

The evolution of the diffraction efficiency of the probing He–Ne laser revealed two major facts: the SRG growth is slower for **AzoDA** than **AzoMe**; the diffraction efficiency saturated after 250 s for **AzoMe** against 1100 s for **AzoDA** (Fig. 9).

This slow growth for **AzoDA** however led to substantially larger diffraction efficiency of 30% against 20% for **AzoMe**. AFM measurements confirmed a higher peak-to-trough amplitude for **AzoDA**, which was found equal to 490 nm compared to 240 nm for **AzoMe**. This unexpected modulation difference is to be related to the initial thickness of the films which were 420 nm for **AzoDA** and 280 nm for **AzoMe**. Since the quantity of azo units, being almost the same, cannot explain this discrepancy, we assumed that each **AzoDA** unit occupied more space than the **AzoMe** due to the bulky backbone of the Diels–Alder substituent. This hypothesis was nicely confirmed by ellipsometry measurements of refractive

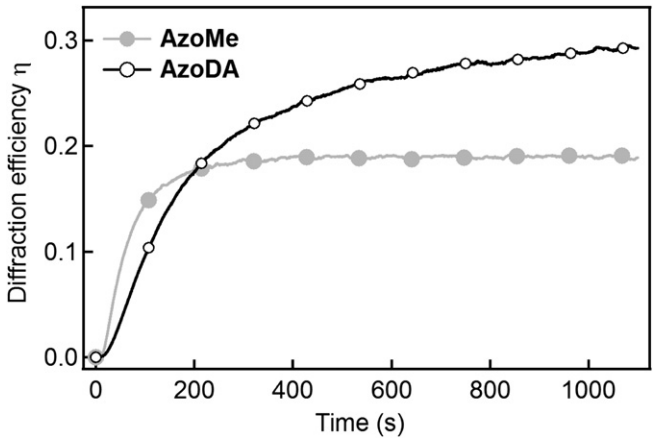

Fig. 9. Comparative inscription dynamics of surface relief gratings onto isoabsorbing azo thins films **AzoMe** and **AzoDA** exposed to two-beam interferential illumination (+45°/−45° polarization configuration; 160 mW cm^{-2} intensity per beam, $\lambda_{irr} = 488$ nm).

indices n, which provided $n = 1.750$ for **AzoDA** and $n = 1.770$ for **AzoMe** at 600 nm. Smaller values of refractive index feature a lower electronic density, which supposes less compact materials as also evidenced in thin films made of triptycenyl-containing semiconductive polymers [33].

Therefore crowded scaffolds do exert steric constraints which slow down the SRG growth but do not inhibit their formation. Another reasonable explanation could be related to the additional mass of bulky substituents, reducing the molecular diffusion coefficient, hence larger photomechanical work is required by the azo units to tow the whole molecular ensemble during their migration process. The apparently paradoxical higher modulation for **AzoDA** despite its crowded molecular structure is related to the large free volume created around each azo unit by the large substituents. After photoisomerization, each azo unit **AzoDA** would free larger space compared to **AzoMe**, since photoisomerization is accompanied with large geometrical modifications. Consequently, migration in **AzoDA** thin films persists and produces even higher surface grating reliefs than those for **AzoMe** samples as it has already been mentioned with other bulky azo molecular glasses [34]. The common statement following which increasing size impedes SRG formation needs to be revisited in the light of the azo geometry, especially when multiple azo units are connected to each other and can respond to light excitation by migrating in a competitive and destructive fashion [23,35].

4. Conclusion

In summary, formation of surface relief gratings in polar azo molecular materials displayed high sensitivity to irradiation conditions (polarization and incident intensity) and structural parameters (thickness and azo bulkiness) as commonly reported for other azo molecular thin films. They however considerably differ in the sense that: first, a +45°/−45° configuration provided more contrasted reliefs than those obtained with a p/p configuration; second, high diffraction efficiency up to 20% was achieved with thin films (270 nm-thick) in less than 200 s by using a low irradiation power (160 mW cm^{-2}); third, the inscription rate of surface relief gratings showed larger sensitivity to film thickness than that observed for polymers (especially over 100 nm), which may be due to the absence of multiple chain interactions with the glass substrate. This latter argument tends to assume that gradient pressure, often evoked for polymeric systems, may not significantly contribute to the migration process within azo molecular glasses. Finally, the appropriate introduction of bulky groups such as anthryl Diels–Alder adduct around the azo chromophores induced a large free volume which is highly beneficial for the azo unit migration. The slower observed growth rate lets us suggest that the rise of SRGs may be described by a cooperative diffusion-based model where the chromophore concentration and the molecular diffusion coefficient along with the photoresponse efficiency need to be considered.

References

[1] Rau H. In: Dürr H, Laurent HB, editors. Photochromism, molecules and systems. Amsterdam Elsevier; 2003. p. 64–164.
[2] Mustroph H, Stollenwerk M, Bressau V. Current developments in optical data storage with organic dyes. Angewandte Chemie, International Edition 2006; 45(13):2016–35.
[3] Natansohn A, Rochon P. Photoinduced motions in azo-containing polymers. Chemical Reviews 2002;102(11):4139–76.
[4] Sekkat Z, Knoll W. Photoreactive organic thin films. San Diego: Academic Press; 2002.
[5] Zhao Y, Ikeda T. Smart light-responsive materials. New Jersey: John Wiley & Sons; 2009.
[6] Delaire JA, Nakatani K. Linear and nonlinear optical properties of photochromic molecules and materials. Chemical Reviews 2000;100(5):1815–47.

[7] Ichimura K, Oh S-K, Nakagawa M. Light-driven motion of liquids on a photo-responsive surface. Science 2000;288:1624–6.
[8] Diguet A, Guillermic R-M, Magome N, Saint-Jalmes A, Chen Y, Yoshikawa K, et al. Photomanipulation of a droplet by the chromocapillary effect. Angewandte Chemie 2009;121(49):9361.
[9] Kausar A, Nagano H, Ogata T, Nonaka T, Kurihara S. Photocontrolled translational motion of a microscale solid object on azobenzene-doped liquid-crystalline films. Angewandte Chemie, International Edition 2009;48:1–5.
[10] Ikeda T, Mamiya J-I, Yu Y. Photomechanics of liquid-crystalline elastomers and other polymers. Angewandte Chemie, International Edition 2007;46:506–28.
[11] Yamada Munenori, Kondo Mizuho, Mamiya Jun-ichi, Yu Yanlei, Kinoshita Motoi, Barrett Christopher J. Photomobile polymer materials: towards light-driven plastic motors. Angewandte Chemie, International Edition 2008;47:4986–8.
[12] Kim DY, Li L, Jiang XL, Shivshankar V, Kumar J, Tripathy SK. Polarized laser induced holographic surface relief gratings on polymer films. Macromolecules 1995;28(26):8835–9.
[13] Barrett CJ, Rochon PL, Natansohn AL. Optically induced surface gratings on azoaromatic polymer films. Applied Physics Letters 1995;66:136–8.
[14] Fiorini C, Prudhomme N, Veyrac Gd, Maurin I, Raimond P. Molecular migration mechanism for laser induced surface relief grating formation. Synthetic Metals 2000;115:121–5.
[15] Lagugné-Labarthet F, Buffeteau T, Sourisseau C. Inscription of holographic gratings using circularly polarized light: influence of the optical set-up on the birefringence and surface relief grating properties. Applied Physics Letters B 2002;74:129–37.
[16] Garrot D, Lassailly Y, Lahlil K, Boilot JP, Peretti J. Real-time near-field imaging of photoinduced matter motion in thin solid films containing azobenzene derivatives. Applied Physics Letters 2009 Jan;94(3):3.
[17] Yager KG, Barrett CJ. Photomechanical surface patterning in azo-polymer materials. Macromolecules 2006;39:9320–6.
[18] Shirota Y. Photo- and electroactive amorphous molecular materials, molecular design, syntheses, reactions, properties, and applications. Journals of Materials Chemistry 2005;15:75–93.
[19] Tanino T, Yoshikawa S, Ujike T, Nagahama D, Moriwaki Kazuyuki, Takahashi T, et al. Creation of azobenzene-based photochromic amorphous molecular materials—synthesis, glass-forming properties, and photochromic response. Journals of Materials Chemistry 2007;17:4953–63.
[20] Nakano H, Takanashi T, Kadota T, Shirota Y. Formation of surface relief grating using a novel azobenzene-based photochromic amorphous molecular material. Advanced Materials 2002;14:1157–60.
[21] Kim M-J, Seo E-M, Vak D, Kim D-Y. Photodynamic properties of azobenzene molecular films with triphenylamines. Chemistry of Materials 2003 09/25; 15(21):4021–7.
[22] Nakano H, Tanino T, Takahashi T, Ando H, Shirota Y. Relationship between molecular structure and photoinduced surface relief grating formation using azobenzene-based photochromic amorphous molecular materials. Journal of Materials Chemistry 2008;18(2):242–6.
[23] Walker R, Audorff H, Kador L, Schmidt HW. Synthesis and structure-property relations of a series of photochromic molecular glasses for controlled and efficient formation of surface relief nanostructures. Advanced Functional Materials 2009;19(16):2630–8.
[24] Priewisch B, Rüch-Braun K. Efficient preparation of nitrosoarenes for the synthesis of azobenzenes. Journal of Organic Chemistry 2005;70(56):2350–2.
[25] Ishow E, Brosseau A, Clavier G, Nakatani K, Pansu RB, Vachon J-J, et al. Two-photon fluorescent holographic rewritable micropatterning. Journal of the American Chemical Society 2007 06/30;129(29):8970–1.
[26] Petti MA, Shepodd TJ, Barrans RE, Dougherty DA. “Hydrophobic” binding of water-soluble guests by high-symmetry, chiral hosts. An electron-rich receptor site with a general affinity for quaternary ammonium compounds and electron-deficient pi-systems. Journal of the American Chemical Society 1988;110:6825–40.
[27] Jacquart A, Tauc P, Nakatani K, Ishow E. Formation of fluorescence reliefs photocontrolled by collective mass migration. Journal of Materials Chemistry 2009;19(47):8999–9005.
[28] Swager TM. Iptycenes in the design of high performance polymers. Accounts of Chemical Research 2008 08/30;41(9):1181–9.
[29] Barrett CJ, Natansohn AL, Rochon PL. Mechanism of optically inscribed high-efficiency diffraction gratings in azo polymer films. The Journal of Physical Chemistry 1996 01/01;100(21):8836–42.
[30] Lee S-H, Balasubramanian S, Kim DY, Viswanathan NK, Bian S, Kumar J, et al. Azo polymer multilayer films by electrostatic self-assembly and layer-by-layer post azo functionalization. Macromolecules 2000 08/01;33(17): 6534–40.
[31] Barrett CJ, Rochon PL, Natansohn AL. Model laser-driven mass transport in thin films of dye-functionalized polymers. Journal of Chemical Physics 1998; 109(4):1505–16.
[32] Lagugné-Labarthet F, Buffeteau T, Sourisseau C. Optical erasures and surface reliefs of holographic gratings inscribed on thin films of an azobenzene functionalised polymer. Physical Chemistry and Chemical Physics 2002;4: 4020–9.
[33] Amara JP, Swager TM. Incorporation of internal free volume: synthesis and characterization of iptycene-elaborated poly(butadiene)s. Macromolecules 2004 03/24;37(8):3068–70.
[34] Ishow E, Camacho-Aguilera R, Guerin J, Brosseau A, Nakatani K. Spontaneous formation of complex periodic superstructures under high interferential illumination of small-molecule-based photochromic materials. Advances Functional Materials 2009;19(5):796–804.
[35] Ueda H, Tanino T, Ando H, Nakano H, Shirota Y. Significant effect of molecular structure on surface relief grating formation for novel azobenzene-based photochromic amorphous molecular materials. Chemistry Letters 2004; 33(9):1152–3.